



Ultra-small gold particles via *Citrus × sinensis*: Theoretical and experimental SERS study

L.F. López-Vázquez^a, L.P. Ramírez-Rodríguez^b, A. Pérez-Rodríguez^a, R. Britto Hurtado^a,
J.L. Cabellos^c, R.A. Vargas-Ortiz^d, A. Navarro-Badilla^b, Manuel A. Roldan^e,
M. Cortez-Valadez^{f,*}

^a Departamento de Investigación en Física, Universidad de Sonora, Apdo. Postal 5-88, 83190 Hermosillo, Sonora, Mexico

^b Departamento de Física, Universidad de Sonora, Apdo. Postal 5-88, 83190 Hermosillo, Sonora, Mexico

^c Universidad Politécnica de Tapachula, Carretera Tapachula a Puerto Madero km 24, San Benito, Puerto Madero, Tapachula, C.P. 30830 Chiapas, Mexico

^d Universidad Autónoma de Sinaloa, Fuente de Poseidón y Prol. Ángel Flores S/N, C.P. 81223 Los Mochis, Sinaloa, Mexico

^e Eyring Materials Center, Arizona State University, Tempe, AZ, USA

^f CONAHCYT-Departamento de Investigación en Física, Universidad de Sonora. Apdo. Postal 5-88, 83190 Hermosillo, Sonora, Mexico

ARTICLE INFO

Keywords:

Ultra-small gold species
Surface enhancement Raman spectroscopy effect
Chemical enhancement mechanism
Charge transfer

ABSTRACT

In this study, we have addressed the green synthesis of sub-nanostructured gold species using *Citrus × sinensis*. Absorption bands in the ultraviolet region (338 nm) were observed. Analysis by atomic resolution microscopy revealed the identification of sub-nanostructured Au species with particle sizes of about 0.9 nm. With favorable results, these systems were tested as substrates for surface-enhanced Raman spectroscopy (SERS) using pyridine. The chemical enhancement mechanism was studied as the source of the SERS effect. Complementarily, the interaction between gold clusters (Au_{2n}, with n = 1–5) and pyridine was modeled using Density Functional at the Becke-3-parameter-Lee-Yang-Parr level of approximation in combination with the LANL2DZ basis set. A correlation between the adsorption energy and the SERS enhancement factor was analyzed as a function of the Au-N interaction distance.

1. Introduction

The current methods for obtaining sub-nanostructured systems or clusters are very scarce. Unlike nanostructured systems, particle size control in subnanodimensional regions presents additional difficulties. Methods involving protecting ligands such as thiols, complex polymers, and DNA have been used to obtain ultra-low-dimensional conjugated particles [1–3]. Such systems have enabled the development of pesticide sensing, metal, and organophosphate detection applications [4–6]. It is due to quantum confinement features and rearrangement of energy levels like molecular systems. Their use has promoted research areas such as energy, environment, electrochemical sensing, and others [7,8].

Such systems have made measuring small species' optical, structural, and vibrational behavior possible. As well as to verify the predictive potential of several approximations in quantum chemistry methodologies. The experimental methods to obtain this ultra-low dimensional system constantly evolve and improve [9,10]. Some studies consider

theoretical analysis to support their experimental hypotheses. In this sense, some authors have achieved to analyze experimental structural parameters that were later correlated with those obtained by theoretical methods within the framework of DFT in the study on rhenium clusters [11]. Additionally, Sufeng An and co-workers have used high-energy ball milling to obtain ultra-small clusters and single iron atoms [12]. For this purpose, a considerable combination of precursors was employed to stabilize the ultra-low-dimensional systems. Complementarily, they analyzed the adsorption energy on specific sites from a DFT perspective. Similarly, experimental methods with a higher degree of complexity have been used to obtain metal clusters. In the case of Yang and co-workers, they used a mass-selected cluster deposition method to obtain Cu clusters/ions in the gas phase using magnetron sputtering [13]. Additionally, they used DFT at the PBE level of approximation to analyze the stability on the Al₂O₃ surface and determine the catalytic activity. On the other hand, green synthesis has been classified as an emerging method focused on synthesizing nanostructured systems,

* Corresponding author.

E-mail address: manuelcortez@live.com (M. Cortez-Valadez).

<https://doi.org/10.1016/j.mseb.2023.116617>

Received 20 September 2022; Received in revised form 16 May 2023; Accepted 28 May 2023

Available online 1 June 2023

0921-5107/© 2023 Elsevier B.V. All rights reserved.

which has been extensively used to obtain particles of a few nanometers. Its capabilities are centered on using phytochemicals to reduce and stabilize metal ions. Many extracts from plants, fruits, leaves, roots, bacteria, and others have obtained several metallic systems, such as gold, silver, copper, platinum, palladium, and more [14–16]. The use of green synthesis to obtain ultra-low-dimensional systems can contribute to essential elements and promising results; however, its use for the stabilization of this type of system has been limited. In this regard, there are reports such as that of Eltaweil and co-workers, where they have used *Atriplex halimus* extract to stabilize platinum particles with minimum sizes of as small as 1.3 nm [17]. Another recent result was obtained by Halawa et al. using pristine β -cyclodextrin as a reductant and stabilizer to obtain gold nanoclusters with minimum particle sizes of 1.5 nm [18]. For both results, the synthesis method yielded an accessible, efficient, competitive, and stable method for obtaining ultra-low-dimensional systems for potential applications.

Additionally, some authors have used *Citrus* \times *sinensis* extract to obtain ultra-small gold nanoparticles through its components. However, the absorption bands in such work were associated with surface plasmon resonance (SPR) in particles larger than 5 nm. Therefore, there was no optical evidence included corroborating the presence of sub-nanostructures [19,20].

Cluster-molecule interaction has provided clues to surface enhancement Raman spectroscopy (SERS) response and allows the study of sub-nanostructured systems [21]. Therefore, density functional theory (DFT) predicts clues of the structural, optical, and electronic parameters of the systems under study due to the contribution of several approximation methods. Today, the experimental study of the SERS effect has diversified but still focuses on Raman activity enhancement of new molecules or not previously studied for their enhancement [22]. Also, there is a notable inclination towards conjugated systems that allow a significant enhancement in Raman activity [23]. Furthermore, using the molecular orbital theory, it is possible to determine the contribution of the charge transfer (CT) factor (or chemical factors such as new molecular electronic states or chemical bond formation) to a specific vibrational mode. A key electronic parameter for this study is the difference between the energy levels of the Highest Occupied Molecular Orbital (HOMO) and Lowest Unoccupied Molecular Orbital (LUMO) of both interacting systems. In this way, it is possible to determine the charge transfer factor associated with a structural affinity state on the cluster-molecule interaction [24].

In this study, *Citrus* \times *sinensis* extract has been used by modifying selected parameters of the synthesis method previously proposed by our group to obtain ultra-small gold clusters (UsAuC) [25]. Experimentally, the optical absorption properties associated with these structures are analyzed. Also, the SERS effect on the pyridine (Py) molecule when interacting with this type of cluster is studied. For providing clues of the structural behavior.

2. Materials and methods

2.1. Synthesis process

Chloroauric acid HAuCl_4 (>99%) by Sigma Aldrich was used as a precursor solution Au^{3+} and *Citrus* \times *sinensis* extract as reducing and stabilizer agent of the particles. Initially, a precursor solution of HAuCl_4 was obtained at 5 mMol. To obtain the extract, we used 1 g of orange pulp in 50 ml of deionized water. The infusion was kept under magnetic agitation at room temperature for 1 h. The solution was filtered and stored for 24 h at room temperature. Subsequently, 1 ml of the precursor solution was added to 30 ml of extract. These were magnetically stirred for 10 min at room temperature.

A UV/VIS spectrophotometer Model VeLab 5100UV was used for the optical absorption study of the gold subnanometer particles, with a resolution of 0.5 nm in the 200–1000 nm range. The TEM/STEM ARM200F at 120–200 kV atomic resolution microscope was used to

obtain high-resolution images of the gold sub-nanostructured systems and to analyze their structural and morphological parameters.

The Raman spectra were recorded using a LabRAM HR Evolution model Raman spectrometer with a 532 nm laser at 5 mW with a resolution of 1 cm^{-1} . The SERS effect was studied on the dry mixture of gold particle solutions (1 ml of gold particle solution and 0.5 ml of pyridine solution with a concentration of 0.5 M) on a glass substrate.

2.2. Computational methodology

Gold clusters were designed Au_{2n} ($n = 1-5$) and optimized to obtain the local minimum energy in the DFT framework at the B3LYP level of approximation (Becke, 3-parameter, Lee–Yang–Parr) in combination with the LANL2DZ base set (Los Alamos National Laboratory 2 Doble-Zeta), integrated in the Gaussian 09 software [26]. Subsequently, the clusters interacted with the Py molecule, then the system was relaxed to the local minimum energy. It allowed us to analyze the modifications of the molecular orbitals before and after the interaction. Implicitly, the energy level of the molecular orbitals in such systems can provide information about the CT mechanism. The adsorption energy was calculated using the local minimum energy associated with each cluster, Py molecule, and the configuration of the interacting system (Supplemental information). To provide a reliable analysis of the active Raman vibrational modes associated with the atomic displacements, Gaussview 06 software was used. Additionally, the points of minimum local energy on the potential energy surface (PES) were corroborated by obtaining only positive frequencies in the vibrational spectra for each case studied.

3. Results and discussion

The optical absorption properties of the UsAuC were analyzed by UV–Vis spectra in the 200–800 nm region, it is shown in Fig. 1. We observed that absorption bands appear near 335 nm at low concentrations of the extract. For similar regions such absorption bands have been associated with the electron transition between molecular orbitals in few-atomic clusters [27]. In addition, Fig. 1 includes the precursor solution (HAuCl_4) showing an absorption band close to 300 nm, attributed to Au^{3+} . It is observed that the UsAuC do not exhibit an absorption band associated with the SPR, which can indicate a molecular nature behavior in sub-nanostructured system.

Atomic Resolution Microscopy images have allowed the structural and morphological properties of the UsAuC to be analyzed. As shown in Fig. 2a, these are distributed without agglomerations. The Atomic

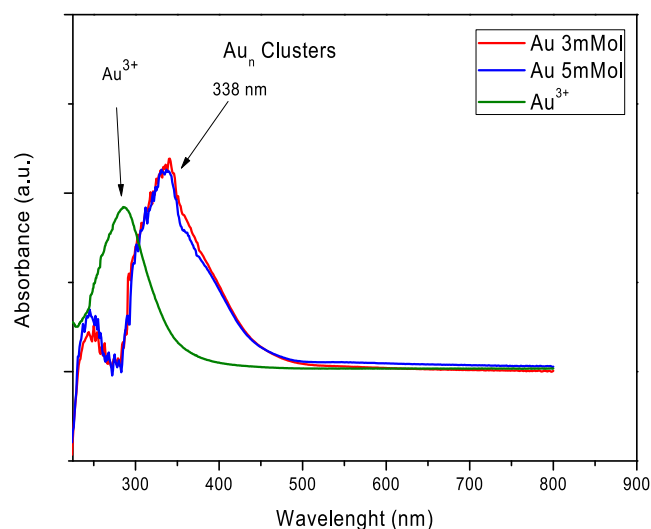


Fig. 1. Optical absorbance spectrum of ion Au^{3+} and Ultra-small Au clusters (UsAuC) obtained with *citrus* \times *sinensis* extract.

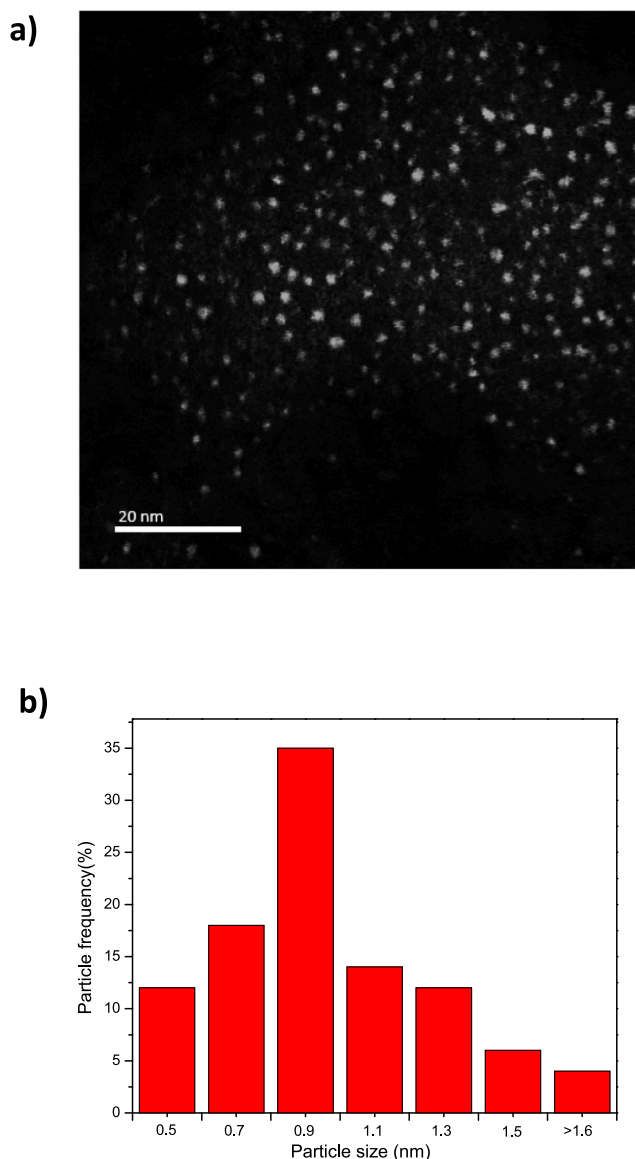


Fig. 2. a) Atomic Resolution Microcopy images of UscAuC and b) particle size histogram from 2a.

Resolution Microscopy image suggests that these clusters comprise only a few tens of atoms. The experimental size of the cluster's ranges from 0.5 nm to 1.5 nm, with a predominant size located at 0.9 nm, as indicated in the particle size histogram in Fig. 2b.

Other synthesis methods used to obtain Au clusters are often associated with processes that involve temperatures below 50 °C [24]. Using *Citrus × sinensis* extract, we replace chemical compounds (some of these with high toxicity) with green components with reducing capacity such as ascorbic acid, glucose, sucrose, starches, flavonoids, terpenoids, proteins, etc. [28]. The green synthesis processes considering room temperature (~300 °K) favor the obtaining of ultra-small Nanoparticles [29]. In other results, gold nanoparticles have been efficiently obtained using *Citrus × sinensis* extract by thermal treatments above 50 °C [30]. However, the particle sizes in the abovementioned study show a trend in the 20–50 nm regions. A generalized mechanism for the early stage of gold particle formation using ascorbic acid (high content in *Citrus × sinensis* extract) is given in Eq. (1). [31].



Where Au(III) represents the gold ions, R represents ascorbic acid, R'

represents an oxidized form of the reductant in this case ascorbate radical and k_1 is the rate constant of the cluster nucleation process.

Furthermore, we have modeled the Py molecule and Au_{2n} gold clusters ($n = 1-5$) under the B3LYP level of approximation in combination with the LANL2DZ basis set to study the structural and optical behavior. As well as provide clues to the structural interaction and charge transfer between these systems. The local minimum energy configurations of these clusters are shown in Fig. 3a. The vibrational spectra were predicted in all cases to verify only positive frequencies to confirm the local minimum energy state. Other authors have reaffirmed the minimum energy configuration for these clusters at different levels of theory [32]. Additionally, the energy level evolution of the HOMO and LUMO molecular orbitals is analyzed for different sizes of gold clusters. The detailed calculations to obtain the molecular descriptors (overall hardness, electronegativity, and adsorption energy) can be found in the Supplemental information.

Complementarily, the experimental Raman spectra of Py and Py-metal clusters interaction are observed in Fig. 4a red and blue line, respectively. The intensification of the Raman activity is observed on the band located at 1050 cm^{-1} associated with the Py ring breathing mode. It is well-known that Py shows Raman activity in all four C_{2v} symmetry classes. The regions of the IR spectrum located between 975 and 1100 cm^{-1} of Py are susceptible to the electromagnetic and CE mechanisms of the SERS effect [33]. The SERS effect in gold nanoparticles is mainly associated with electromagnetic factors on the surface of the nanoparticles, the main contribution due to the resonance of the surface, with an amplification order of approximately 10^7 . According to the proposed method, it was possible to obtain gold species with a few tens of atoms. In such systems, there are other contribution, as CE mechanism, which are generally related to the energy levels of the HOMO and LUMO. The CE has a lower impact on the SERS effect compared to the electromagnetic mechanism. However, its enhancement factor contributes up to 10^4 . For the SERS study, the Py molecule is considered in interaction with metal clusters after the subsequent relaxation of both systems (Fig. 3b). The energy levels of the HOMO-LUMO before and after the Au_n -Py interaction are included in the supplemental information. From these results, we obtained that the interaction distance of the Au_n clusters with the Py molecule ranges between 2.1 and 2.3 Å (N-Au). We find some affinity for the nitrogen atom in all cases.

In addition, we suppose that a rearrangement of the energy levels of the HOMO-LUMO after the interaction could enhance the SERS effect. As well as improving the degree of CT. All Raman spectra were predicted after interaction with the Au_n clusters Fig. 4b. From these spectra, it is observed that the main band located at 1021.9 cm^{-1} presents an enhancement. This vibrational mode is associated with the hexagonal ring breathing of Py. To quantify the SERS effect between the metal species and the Py, the integrated Raman specific enhancement factor (SEF) is defined. This SEF factor is calculated with the expression (1).

$$\text{SEF} = \frac{\sum I_{SERS}^{\text{Py}}}{\sum I_{Raman}^{\text{Py}}} \quad (1)$$

Were I_{SERS}^{Py} corresponds to the intensities summation of vibrational modes associated with Py in the system comprising Au_n -Py and I_{Raman}^{Py} corresponds to the intensities summation in the vibrational modes associated with isolated Py. The SEF values are relevant as it quantifies the intensity in the Raman spectrum of the molecule. For this purpose, all the modes present in the molecule are considered, neglecting those associated with the cluster-Py interaction. For gold species, Raman active modes are regularly observed up to about 350 cm^{-1} [34]. The SEF values are listed in Table 1, highlighting that Au_8 is the cluster with the highest SEF. For the Au_2 and Au_8 clusters, the highest enhancement in the vibrational band associated with the radial breathing of the Py ring is observed. For the Au_4 and Au_{10} clusters, the increase in this vibrational mode was minimal relative to the Raman spectrum of the isolated Py molecule. Additionally, another important parameter is the electron

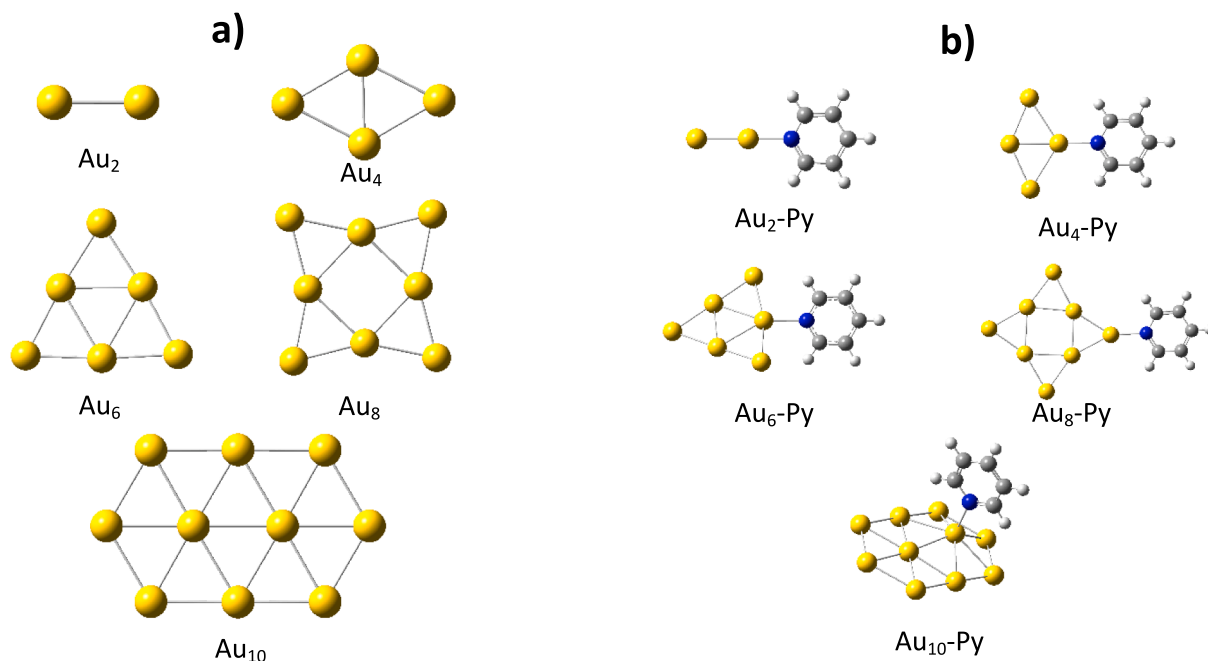


Fig. 3. DFT calculations: a) Lowest energy configurations of Au_{2n} (n = 1–5) clusters and b) Au_{2n}-Py interaction.

transfer fraction (ΔN). This parameter is related to electronegativity and global hardness and is represented by Pearson's Method as:

$$\Delta N = \frac{\chi_{cluster} - \chi_{pyridine}}{2[\eta_{cluster} + \eta_{pyridine}]} \quad (2)$$

with $\chi_{cluster}$ and $\eta_{cluster}$ as electronegativity and overall hardness parameters for the cluster, and $\chi_{pyridine}$ and $\eta_{pyridine}$ as the respective parameters for the molecule. The difference in the numerator, or the difference in electronegativities, will be responsible for the transfer of electrons. This process will occur from the molecule with a low electronegativity to the molecule with higher electronegativity [24]. (Supplemental information)

An important parameter is the adsorption energy, and it was defined as the energy of the molecule to adsorb atoms or clusters on its surface. This parameter can be considered as a criterion of the system stability, which is calculated based on the following relationship:

$$E_{ads} = -\{E(Cluster + Pyridine) - [E(Pyridine) + E(Cluster)]\} \quad (3)$$

with $E(Cluster + Pyridine)$ as the local minimum energy of the system comprising the cluster and the Py molecule, $E(Pyridine)$ as the local minimum energy of the isolated Py and $E(cluster)$ the local minimum energy of the isolated cluster. This parameter indicates that the molecule can bind the cluster. With high values, the cluster-molecule system will be considered more stable [35]. Considering the values obtained for the local minimum energies of the cluster- Py systems and using equation (1), the adsorption energies (E_{ads}) are obtained in Table 1. It is observed that the maximum value is obtained for the system composed of Au₄-Py. Hence, the interaction of Py with the Au₄ cluster exhibits higher stability in this system. Otherwise, when considering the Au₁₀ interaction, a minimum adsorption value is obtained.

The calculations on the interaction of Py with the Au_{2n} clusters allowed us to determine the behavior of the SEF and Eads, considering the distance between the nitrogen atom of the Py and the nearest gold atom. At first approximation, we observe (Fig. 5) that the adsorption energy presents an almost linear and inversely proportional decrease to the N-Au separation. On the other hand, the SEF could present a

Gaussian-like behavior, suggesting a maximum value close to the experimentally reported distance for the N-Au interaction.

4. Conclusion

Gold sub-nanostructured systems were obtained using the green synthesis method with *Citrus × sinensis* extract. The analysis through Atomic Resolution Microscope allowed the identification of sub-nanometric gold particles with a size of around 0.9 nm. An absorption band was found and associated with electronic transitions in gold clusters by UV/Vis spectroscopy located in 338 nm. DFT calculations of Py and Au clusters allowed the study of electronegativity and global hardness. In addition, the study of the electron transfer fraction between the two molecular systems allowed us to find that Au₂-Py has the highest electron transfer fraction. Therefore, these results suggested that the CE mechanism is responsible for the experimental Raman spectrum enhancement. The difference between HOMO-LUMO orbitals revealed a trend to decrease as the size increases of the metal cluster. As well as a subsequent HOMO-LUMO decrease after interaction with the Py molecule. The relationship between the electronegativity and the global hardness of the modeled systems allowed us to corroborate the degree of charge transfer contribution and its relationship with other chemical bonding factors responsible for the SERS effect. The charge transfer contribution degree was ranged from 0.12 – 0.18 for the modeled systems. The SERS effect reveals a dependence on the interaction distance between the Py and metal cluster systems, indicating a maximum enhancement close to the experimentally reported value for the N-Au bond (2.17 Å in this study).

5. Data availability statement

The raw/processed data required to reproduce these findings are available on request to corresponding author M. Cortez-Valadez.

Declaration of Competing Interest

The authors declare that they have no known competing financial interests or personal relationships that could have appeared to influence

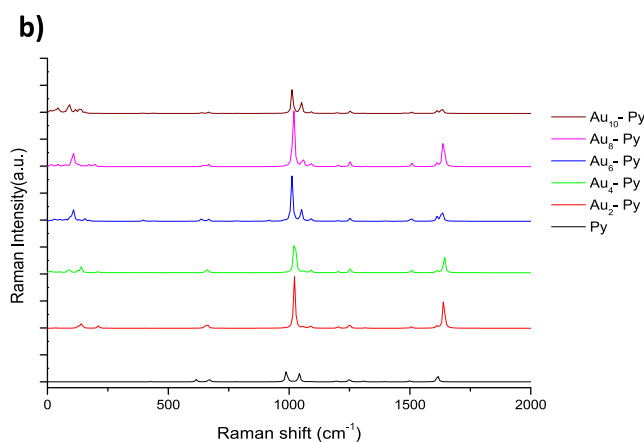
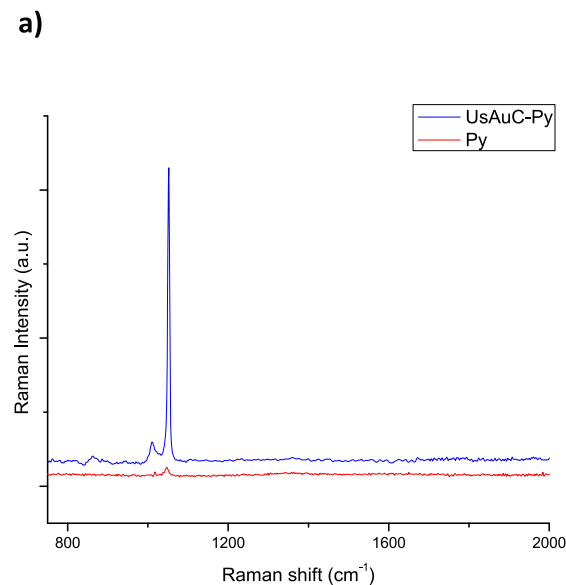


Fig. 4. Raman spectra of a) experimental Py-UsAuC and b) theoretical: Au_{2n}-Py modeled systems.

Table 1
Molecular descriptors predicted after Au_n-Py interaction.

System	HOMO (eV)	LUMO (eV)	Bond (Au-N)	Electron Transfer Fraction (ΔN)	E _{ads} (eV)	Specific Enhancement Factor*
Au ₂ -Py	-5.71	-2.33	2.14	0.18	1.29	1.38
Au ₄ -Py	-5.43	-2.60	2.13	0.16	1.36	1.20
Au ₆ -Py	-5.75	-3.05	2.30	0.13	0.46	1.49
Au ₈ -Py	-5.93	-3.12	2.17	0.12	1.03	1.76
Au ₁₀ -Py	-5.86	-3.63	2.31	0.15	0.35	1.11

* Raman enhancement factor on Pyridine vibrational modes.

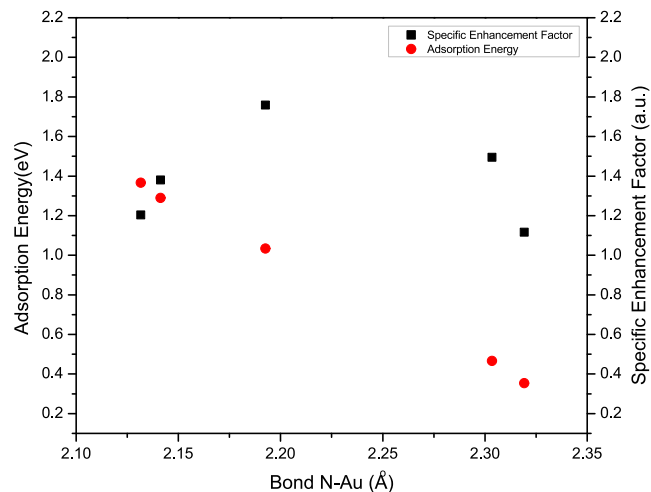


Fig. 5. Relationship of adsorption energy, SEF, and N-Au bind interaction in the Au_{2n}-Py systems calculated at lowest energy configurations.

the work reported in this paper.

Data availability

Data will be made available on request.

Acknowledgements

This work was supported by A1-S-46242 project of the CONAHCYT Basic Science. The author M. Cortez-Valadez appreciates the support by “Investigadores por México” program. We acknowledge the use of facilities within the Eyring Materials Center at Arizona State University supported in part by NNCI-ECCS-1542160. R. Britto Hurtado acknowledges to Postdoctoral Fellowship by CONAHCYT Mexico.

Appendix A. Supplementary data

Supplementary data to this article can be found online at <https://doi.org/10.1016/j.mseb.2023.116617>.

References

- [1] C.I. Richards, S. Choi, J.C. Hsiang, Y. Antoku, T. Vosch, A. Bongiorno, Y.L. Tzeng, R.M. Dickson, *J. Am. Chem. Soc.* 130 (2008) 5038.
- [2] J.M.J. Fréchet, *Science* 263 (1994) 1710.
- [3] Q. Huifeng, L. Chao, J. Rongchao, *Sci. China Chem.* 55 (2012) 2359.
- [4] F. Zhao, J. Wu, Y. Ying, Y. She, J. Wang, J. Ping, *TrAC Trends Anal. Chem.* 106 (2018) 62.
- [5] E. Bolli, A. Mezzi, L. Burratti, P. Proposito, S. Casciardi, S. Kaciulis, *Surf. Interface Anal.* 52 (2020) 1017.
- [6] Q.J. Luo, Z.G. Li, J.H. Lai, F.Q. Li, P. Qiu, X.L. Wang, *RSC Adv.* 7 (2017) 55199.
- [7] X. Gao, S. He, C. Zhang, C. Du, X. Chen, W. Xing, S. Chen, A. Clayborne, W. Chen, X.H. Gao, S.J. He, C.M. Zhang, C. Du, W. Xing, W. Chen, X. Chen, A. Clayborne, S. L. Chen, *Adv. Sci.* 3 (2016) 1600126.
- [8] A. Aparna, H. Sreehari, A. Chandran, K.P. Anjali, A.M. Alex, P. Anuvinda, G. B. Gouthami, N.P. Pillai, N. Parvathy, S. Sadanandan, A. Saritha, *Talanta* 239 (2022), 123134.
- [9] A.A. Al-Saadi, M. Haroon, S.A. Popoola, T.A. Saleh, *Sens. Actuators B Chem.* 304 (2020), 127057.
- [10] T.A. Saleh, K.M.M. AlAqad, A. Rahim, *J. Mol. Liq.* 256 (2018) 39.
- [11] O. Miramontes, F. Bonafé, U. Santiago, E. Larios-Rodriguez, J.J. Velázquez-Salazar, M.M. Mariscal, M.J. Yacaman, *Phys. Chem. Chem. Phys.* 17 (2015) 7898.
- [12] S. An, G. Zhang, T. Wang, W. Zhang, K. Li, C. Song, J.T. Miller, S. Miao, J. Wang, X. Guo, *ACS Nano* 12 (2018) 9441.
- [13] B. Yang, C. Liu, A. Halder, E.C. Tyo, A.B.F. Martinson, S. Seifert, P. Zapol, L. A. Curtiss, S. Vajda, *J. Phys. Chem. C* 121 (2017) 10406.
- [14] T.A. Saleh, M.M. Al-Shalalfeh, A.T. Onawole, A.A. Al-Saadi, *Vib. Spectrosc.* 90 (2017) 96.
- [15] T.A. Saleh, *Environ. Technol. Innov.* 20 (2020), 101067.
- [16] T.A. Saleh, *Environ. Technol. Innov.* 24 (2021), 101821.

- [17] A.S. Eltaweil, M. Fawzy, M. Hosny, E.M. Abd El-Monaem, T.M. Tamer, A.M. Omer, *Arab. J. Chem.* 15 (2022), 103517.
- [18] M.I. Halawa, F. Wu, T.H. Fereja, B. Lou, G. Xu, *Sens. Actuators B Chem.* 254 (2018) 1017.
- [19] B. Yang, F. Qi, J. Tan, T. Yu, C. Qu, *Appl. Sci.* 9 (2019) 2423.
- [20] M.A. Islam, *J. Chem. Soc. Pak.* 4 (2015) 721.
- [21] Y. Ye, H. Bai, W. Liu, Y. Li, M. Yu, J. Li, G. Xi, *ChemistrySelect* 5 (2020) 3105.
- [22] M. Dendisová, Z. Němečková, M. Člupek, V. Prokopec, *Appl. Surf. Sci.* 470 (2019) 716.
- [23] D. Zhang, H. You, L. Yuan, R. Hao, T. Li, J. Fang, *Anal. Chem.* 91 (2019) 4687.
- [24] S.K. Saha, P. Ghosh, A. Hens, N.C. Murmu, P. Banerjee, *Phys. E Low-Dimensional Syst. Nanostruct.* 66 (2015) 332.
- [25] M. Cortez-Valadez, L.P. Ramírez-Rodríguez, F. Martínez-Suarez, R.A. Vargas-Ortiz, F.F. Castellón-Barraza, M. Flores-Acosta, *J. Inorg. Organomet. Polym. Mater.* 31 (2021) 1079.
- [26] M.J. Frisch, G.W. Trucks, H.B. Schlegel, G.E. Scuseria, M.A. Robb, J.R. Cheeseman, G. Scalmani, V. Barone, B. Mennucci, G.A. Petersson, H. Nakatsuji, M. Caricato, X. Li, H.P. Hratchian, A.F. Izmaylov, J. Bloino, G. Zheng, J.L. Sonnenberg, M. Hada, M. Ehara, K. Toyota, R. Fukuda, J. Hasegawa, M. Ishida, T. Nakajima, Y. Honda, O. Kitao, H. Nakai, T. Vreven, J.A. Montgomery Jr., J.E. Peralta, F. Ogliaro, M. Bearpark, J.J. Heyd, E. Brothers, K.N. Kudin, V.N. Staroverov, R. Kobayashi, J. Normand, K. Raghavachari, A. Rendell, J.C. Burant, S.S. Iyengar, J. Tomasi, M. Cossi, N. Rega, J.M. Millam, M. Klene, J.E. Knox, J.B. Cross, V. Bakken, C. Adamo, J. Jaramillo, R. Gomperts, R.E. Stratmann, O. Yazyev, A.J. Austin, R. Cammi, C. Pomelli, J.W. Ochterski, R.L. Martin, K. Morokuma, V.G. Zakrzewski, G.A. Voth, P. Salvador, J.J. Dannenberg, S. Dapprich, A.D. Daniels, Ö. Farkas, J.B. Foresman, *Orti. Gaussian* 09, Revis. E.01.
- [27] I. Tuzovskaya, N. Bogdanchikova, A. Simakov, V. Gurin, A. Pestryakov, M. Avalos, M.H. Farías, *Chem. Phys.* 338 (2007) 23.
- [28] S. Ying, Z. Guan, P.C. Ofoegbu, P. Clubb, C. Rico, F. He, J. Hong, *Environ. Technol. Innov.* 26 (2022), 102336.
- [29] M. Celentano, A. Jakhmola, M. Profeta, E. Battista, D. Guarnieri, F. Gentile, P. A. Netti, R. Vecchione, *Colloids Surf. A Physicochem. Eng. Asp.* 558 (2018) 548.
- [30] M.V. Sujitha, S. Kannan, *Spectrochim. Acta Part A Mol. Biomol. Spectrosc.* 102 (2013) 15.
- [31] T.A. Saleh, M.M. Al-Shalalfeh, A.A. Al-Saadi, *Sci. Rep.* 6 (2016), 32185.
- [32] P.K. Jain, *Struct. Chem.* 16 (2005) 421.
- [33] E. Dumont, C. De Bleye, M. Haouchine, L. Coïc, P.Y. Sacré, P. Hubert, E. Ziemons, *Spectrochim. Acta Part A Mol. Biomol. Spectrosc.* 233 (2020), 118180.
- [34] S.M. Morton, L. Jensen, *J. Am. Chem. Soc.* 131 (2009) 4090.
- [35] S.K. Saikin, R. Olivares-Amaya, D. Rappoport, M. Stopa, A. Aspuru-Guzik, *Phys. Chem. Chem. Phys.* 11 (2009) 9401.